

EFFECT OF MOLTEN SALT PROPERTIES ON INTERNAL FLOW AND DISK FRICTION LOSS OF MOLTEN SALT PUMP

by

**Yong-Xin JIN^a, De-Sheng ZHANG^{a*}, Xi SHENG^a, Lei SHI^a,
Wei-Dong SHI^{a,b}, and Dao-Hong WANG^c**

^a Research Center of Fluid Machinery Engineering and Technology, Jiangsu University,
Zhenjiang, Jiangsu, China

^b School of Mechanical Engineering, Nantong University, Nantong, Jiangsu, China

^c Jiangsu Feiyue Machine and Pumps Group Co., Ltd. Taizhou, Jiangsu, China

Original scientific paper

<https://doi.org/10.2298/TSCI2004347J>

Computational fluid dynamics is used to study the effect of temperature on flow structure and disk friction loss for different working fluids in a high temperature molten salt pump, which is used for concentrating solar power, the velocity profile and pressure distribution in the first stage of the pump model and the effect of the fluid property on the ring leakage, disk friction loss as well as the shear stress distribution on shroud are analyzed for the pure water and the molten salt with temperature 300 °C and 565 °C, respectively. The main findings can be concluded as: the working fluids have little effect on pump performance and internal velocity distribution whereas the pressure of the flow field would increase with the fluid density, with the increase of the fluid viscosity, the shear stress inside the ring also increases and the total leakage can be eliminated evidently, the increase of the fluid density and viscosity show the significant responsibility for the disk friction loss, in which the fluid viscosity also increases the disk friction loss, and the viscosity is one of the most influential factors for the shroud shear stress and it can be observed that the shear stress on front shroud is higher than that on the rear shroud. It is believed that the present work can deep the understandings of the fluid structures inside the molten salt pump, which can provide some guidelines to improve the pump performance and optimize the pump structure.

Key words: molten salt pump, concentrating solar power, medium properties, disk friction loss

Introduction

Molten salt pump (MSP), as an essential power equipment in chemical and metallurgical processes, is often used in a new generation of nuclear power, concentrating solar power (CSP), energy storage and other important energy facilities. It is always utilized in CSP system and there has some specialities in the mechanical structure and transporting medium characteristics [1]. The function and working environment of the MSP in different positions in the molten salt energy circulatory system are quite different, resulting in some differences in pump structure and environmental conditions [2]. Therefore, the flow structure, disk friction loss and pump performance of the molten salt under different temperature conditions are necessary to be studied, for improving the design of the MSP by the obtained computational results.

* Corresponding author, e-mail: zds@ujs.edu.cn

In CSP system, binary nitrates are used in the molten salt circulatory system and the temperature has a great impact on molten salt physical characteristics [3-6]. The change of molten salt properties will affect the performance of the pump at different temperatures significantly [7]. For some specific examples, Cheng *et al.* [8] analyzed the influence of viscosity on the flow characteristics of MSP under different temperature conditions and obtained the instantaneous flow field distributions. Xiao *et al.* [9] used five kinds of molten salts with different densities and similar viscosity to analyze the effect of density on pump performance. Daily *et al.* [10] analyzed the the external characteristics and the flow characteristics in centrifugal pumps for different viscous media based on the SST $k-\omega$ turbulence model. Li [11] obtained the velocity distribution of the impeller under the optimal condition for the oil and pure water by LDV measurements and the flow separation and velocity distribution of the impeller were studied in detail.

According to the aforementioned investigations, less attention is paid to the flow structures inside the MSP for CSP systems under different temperature conditions [12-14]. In this work, with the various temperature, the detailed flow field and pump performance under the rated condition are studied systematically by the numerical simulations.

Physical model and mesh generation

Physical model

The three-stage model pump with guide vanes has a long axis, and the basic geometrical parameters at design point are listed as follows: head $H = 150$ m, flow rate $Q_d = 350$ m³/h, rotating speed $n = 1450$ rpm. A large impeller side chamber clearance is set to ensure that the impeller shroud and the guide vane component cannot interfere each other, and the details are presented in fig. 1. The whole flow field will be simulated and the modeling domain is the first stage impeller side chamber.

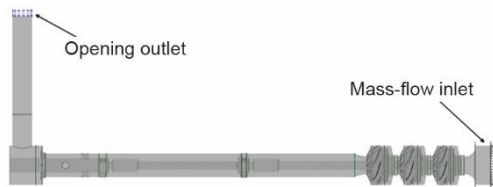


Figure 1. Calculation domain and boundary conditions

Grid independence

The mesh quality has a great influence on the flow field and performance prediction. In order to obtain better convergence with the affordable computational resources, the pump calculated domain adopts high-quality hexagonal structured grid. According to the grid independence results shown in tab. 1, it can be seen that the number of the grid increases but the efficiency tends to be stable. Therefore, the total grid number approximately $24.8 \cdot 10^6$ is selected in the computations. The detailed mesh information of various hydraulic components are shown in fig. 2.

Table 1. Grid independence results

Grid number	Nodes	H [m]	η [%]
$12.5 \cdot 10^6$	$13.3 \cdot 10^6$	152.22	68.18
$24.8 \cdot 10^6$	$25.2 \cdot 10^6$	151.8	67.93
$28.5 \cdot 10^6$	$28.9 \cdot 10^6$	151.75	67.87

Numerical set-up and experimental result

Turbulence model and boundary condition

The SST $k-\omega$ turbulence model was selected to investigate the flow structure in MSP. For SST $k-\omega$ turbulence model combines the advantages of both $k-\omega$ model and $k-\epsilon$ model and it can be a very good treatment for the near-wall flows. A classical boundary condition is adopted: the mass-flow rate is imposed on the inlet section and the pressure is assigned at the opening outlet according to the operating condition, which was shown in fig. 1. The impeller is set as rotating domain, which has the rotation speed $n = 1450$ rpm, and the other static hydraulic components are set as no slip walls. The frozen-rotor model is used for the interface between the rotating domains and the stationary parts.

The working fluids are pure water, molten salt at 300° and molten salt at 565° , respectively. The law of the physical change of the molten salt is determined by the literature [3] shown in fig. 3.

Experimental set-up and numerical results

As is shown in fig. 4, the test rig is a typical open-type test system, which is composed of the data acquisition instrument and pipeline system. The test and calculated results are presented in fig. 5. The tested range is $(0-1.6)Q_d$, Q_d is the design flow rate, while the five operating conditions for the numerical simulations are in the range of $(0.4-1.1)Q_d$. By the comparison of the pump performance, it is observed that the calculated head is higher than the experiment by 3.93% for the pure water, 5.87% for the salt melt at 300°C and 4.69% for the salt melt at 565°C . Simultaneously, the density and viscosity have little effect on the pump performance under the rated condition, which agrees well with the conclusions in references [8, 9, 11]. Due to the small difference of the pump performance when the working fluid changes, the initial design of the hydraulic model and the performance can be referred to which of pure water.

In present work, the effect of the medium physical parameters on pump performance and flow structures are obtained. Among three different working fluids, the density of molten salt at 300°C and 565°C are quite close and the viscosity of molten salt at 565°C and the

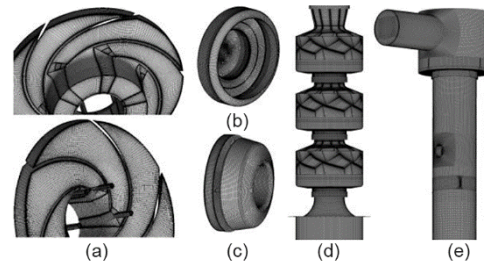


Figure 2. Mesh generation for the pump model; (a) impeller, (b) front impeller room, (c) rear impeller room, (d) suction stage, (e) discharge casing

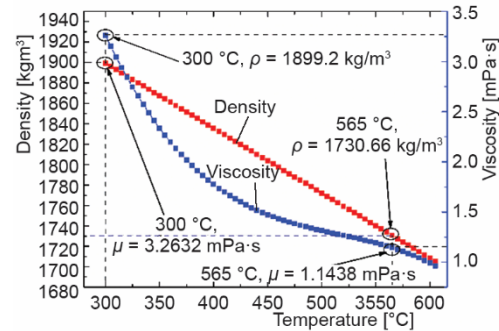


Figure 3. Property curves of the medium

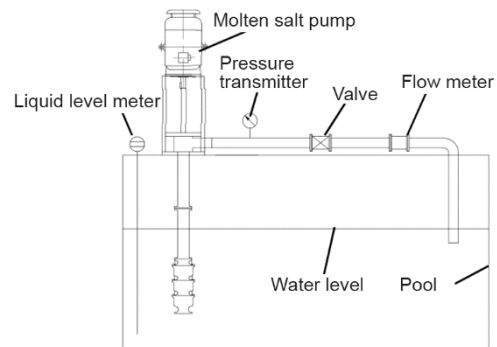


Figure 4. Test rig

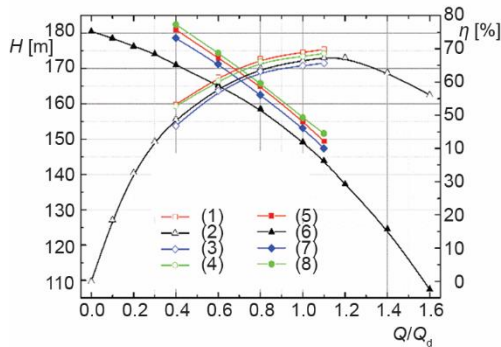


Figure 5. Experimental and numerical results;
1 – CFD η (water), 2 – EXP η (water), 3 – CFD η
(300 °C molten salt), 4 – CFD η (565 °C molten salt),
5 – CFD H (water), 6 – EXP H (water), 7 – CFD H
(300 °C molten salt), 8 – CFD H (565 °C molten salt)

relative streamline length interval of 0.5-1.0, and the largest magnitude occurs at the outlet throat of the flow channel.

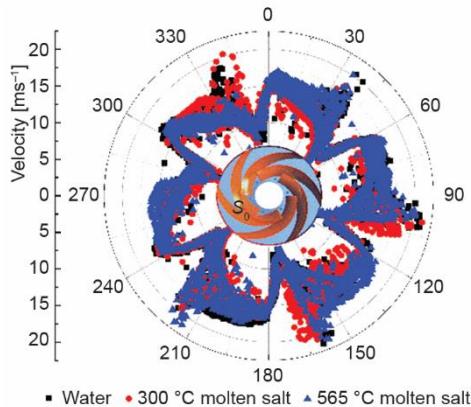


Figure 6. Relative velocity distribution at the impeller outlet

The average relative velocity at the impeller outlet for the pure water, molten salt at 300 °C and at 565 °C is 13.30 m/s, 13.05 m/s, and 13.38 m/s, and it is approximately 10.85 m/s, 10.83 m/s, and 10.98 m/s inside the impeller, respectively. It seems that there has little difference in average relative velocity among three media. The average relative velocity and velocity distribution show that the large viscosity leads to a relatively low velocity. The overall trend of the velocity distribution is not affected by the density and viscosity, but the local velocity distribution varies with the physical properties. Among three media, the viscosity of the pure water and molten salt at 565 °C is extremely close while the viscosity of molten salt at 300 °C is about 3 times than that for the other two ones, indicating that the viscosity difference is the main reason for the relative velocity change.

The impeller outlet pressure of the pure water, molten salt at 300 °C and at 565 °C in different distribution intervals are shown in figs. 8 and 9. The impeller outlet pressure and

pure water are also very similar. Consequently, the influence of the viscosity and the density on the flow field and pump performance can be achieved by the comparisons of these three medium.

Results and discussion

Flow structures in impeller

The distribution of relative velocity inside the first stage impeller is shown in figs. 6 and 7. In the impeller, the trend of relative velocity distribution for the three medium is almost the same. It is observed that the relative velocity for the pure water agrees well with that for molten salt at 565 °C. The difference in relative velocity mainly exists on

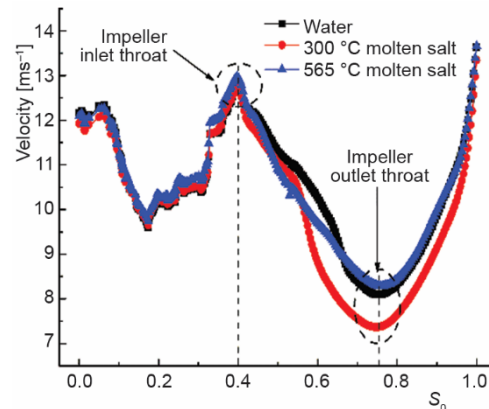


Figure 7. Relative velocity distribution in impeller; S_0 is the relative streamline position

blade outlet pressure are similar for molten salt at 300 °C and at 565 °C, whereas these parameters for the pure water are quite different with the other two media. The average static pressure at impeller outlet for three different media are 3936615.6 Pa, 752540.1 Pa, and 689333.1 Pa and the pressure ratio is 1:1.91:1.75. The maximum pressure on the blade surface are 456791.1 Pa, 850182.4 Pa, and 796714.4 Pa and the ratio is 1:1.86:1.74. The ratio of the pressure on impeller outlet to the maximum pressure of blade are close to the medium density ratio: 1:1.9:1.73. Therefore, it can be seen that the medium density is the key factor affecting the flow field pressure.

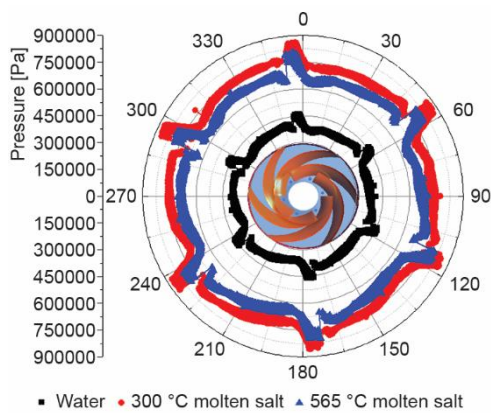


Figure 8. Pressure at the impeller outlet

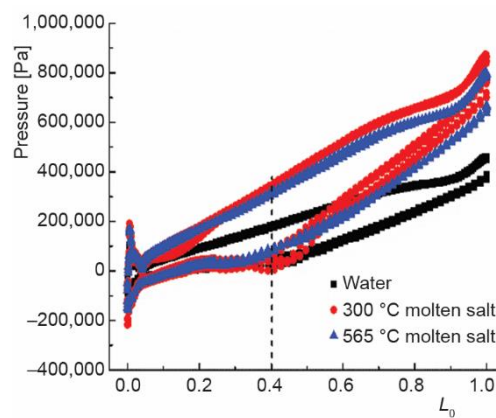


Figure 9. Pressure distribution on blade surface; L_0 is the relative length of blade

Flow structures and leakage inside the ring gap

The influence of the clearance and the clearance flow on the flow field are analyzed in detail in references [15-17]. The conclusion indicated that the flow in the clearance has a great influence on the performance and flow characteristics of the pump. Figure 10 is a diagram of the position for each section in the gap. P1, P2, and P3 are the sections on the front ring gap while P4 and P5 are the sections on the back ring gap.

Figures 11 and 12 show the distributions of the shear strain rate and shear stress in different sections of the gap for three media under designed condition. The largest discrepancy is mainly on the minimum radius and the maximum radius of the wall surface. However, the shear stress of each section is greatly affected by the physical properties of the medium. The viscosity of the pure water and molten salt at 565 °C are quite similar and the density of molten salt at 300 °C and at 565 °C are also the same. By comparing the distribution of the shear stress, it can be seen that the viscosity is the dominant factor affecting the shear stress.

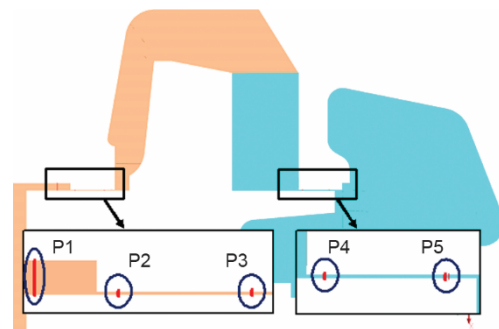


Figure 10. Cross-sections of the ring gap

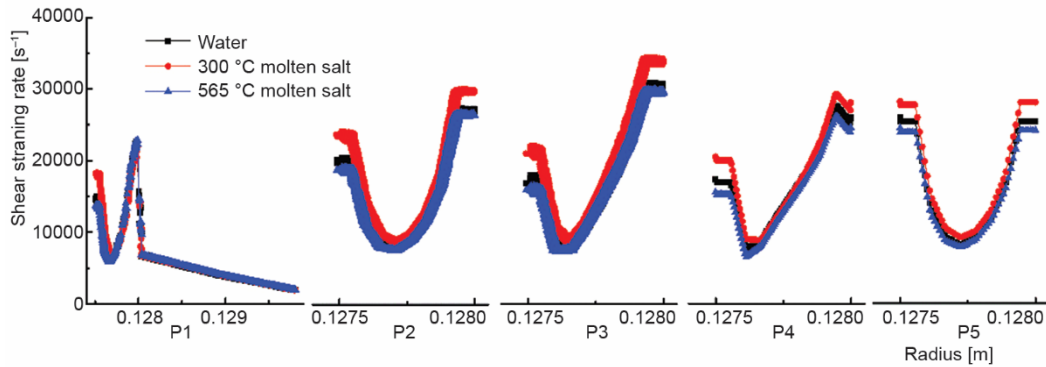


Figure 11. Distributions of the shear strain rate at ring planes, ratio order: water, molten salt at 300 °C, and molten salt at 565 °C

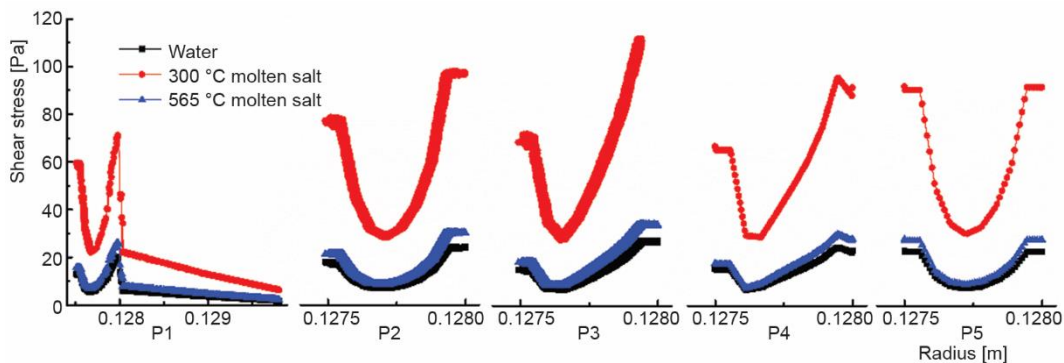


Figure 12. Distributions of the shear stress at ring planes

As can be seen from tab. 2, the shear strain rates and their ratios of the sections are close each other for three media. The phenomena show that the influence of density and viscosity on shear strain rate is small, and this conclusion confirms that the influence of density and physical properties on the velocity is relatively weak. Meanwhile, the shear stress ratio of the five sections is comparatively consistent. The ratios for the clear water, molten salt at 565 °C and molten salt at 300 °C become large gradually.

Table 2. The ratio of statistics on sections

Section	Shear strain rate	Shear stress
P1	1:1.12:1.01	1:4.10:1.30
P2	1:1.11:0.98	1:4.07:1.26
P3	1:1.11:0.98	1:4.01:1.26
P4	1:1.09:0.93	1:4.01:1.20
P5	1:1.10:0.95	1:4.02:1.22

The leakage volume will also vary considerably for different media under designed condition, as is shown in fig. 13. The leakage volume ratio of three different media for the front

ring and the rear ring are 1:1.01:1.02 and 1:0.94:0.96 while the total leakage volume ratio is 1:0.97:0.99. There is little difference in front ring leakage, rear ring leakage and total leakage, and the total leakage volume is opposite to the viscosity distribution. Therefore, the main factors affecting leakage are the medium density and viscosity. According to the analysis of the leakage, the design of the MSP gap only needs to consider the deformation caused by the high temperature.

The disk loss analysis

The energy of the medium's rotating motion in pump chamber comes from the viscosity, which leads to the disk friction loss. The geometry of the pump chamber and the characteristics of the medium determine the disk friction loss. The influence of the physical property change caused by temperature variations on disk friction loss is the focus for present research.

According to the information shown in fig. 14, the energy loss of the front and rear shroud is consistent with the medium density and the viscosity. The energy of the disk friction loss is: 2264.7 W, 4992.7 W, and 3590.4 W, and its ratio is 1:2.20:1.59. The percentage of disk friction loss for the clear water, molten salt at 300 °C and molten salt at 565 °C is 11.2%, 17.5%, and 10.3%, respectively. The percentage of disk friction loss for the clear water and molten salt at 565 °C is very close, but the value of the disk friction loss for the molten salt at 300 °C with higher viscosity is significantly higher than that of the other two media, indicating that the percentage of energy loss will increase with the viscosity.

In this model, the circumferential velocity distribution of the pump chamber agrees with the results in reference [18]. The volume of the back shroud chamber is about 1.8 times than that of the front shroud chamber, so the energy required for the medium rotation in the back shroud chamber is higher than that of the front shroud chamber. For this reason, the energy loss of the back shroud is higher than that of the front shroud. The velocity distribution of the flow field does not change much for different media, so the disk friction loss is mainly affected by the density and viscosity of the medium. The increase in density inevitably leads to an increase in disk friction loss, but the magnitude of the energy loss is not proportional to the density, and it can be seen that the viscosity has a certain influence on the disk friction loss.

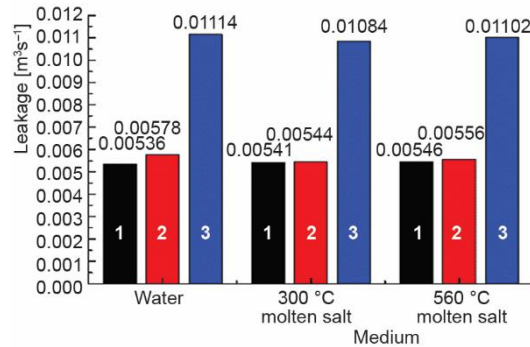


Figure 13. Leakage in the ring gap; 1 – front ring gap leakage, 2 – back ring gap leakage, 3 – total leakage

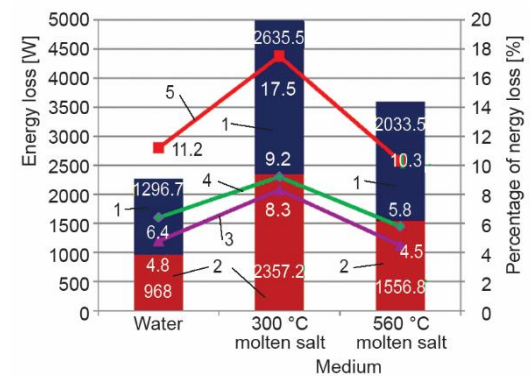


Figure 14. Energy loss; 1 – rear shroud energy loss, 2 – front shroud energy loss, 3 – front shroud energy loss as a percentage of total energy loss, 4 – rear shroud energy loss as a percentage of total energy loss, 5 – disk friction loss as a percentage of total energy loss

Shear strain rate and stress distributions of the shroud

The shear strain rate and shear stress on shroud are shown in figs. 15 and 16 and the results reveal that the trend of the distributions for three media are consistent. Due to the

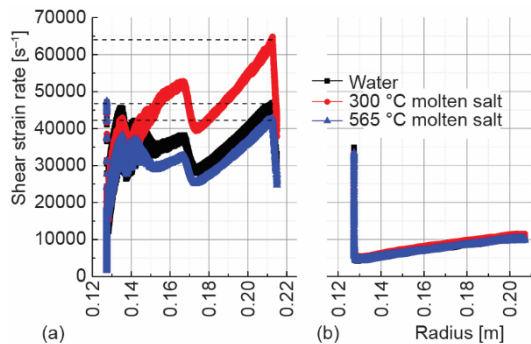


Figure 15. Distributions of the shear strain rate on shroud; (a) shear strain rate on front shroud, (b) shear strain rate on rear shroud

complex geometry of the front cover cavity, the shear strain rate and stress region of the front shroud changes abruptly. Figure 14 indicates that the mutation region and geometry are strongly correlated, and the mutation significantly increases the shear strain rate and shear stress on the shroud. The shear strain rate and shear stress on the rear shroud are regular and the magnitude of which on the front shroud are higher than that on the rear shroud. The fluid interacts with the junction by the impeller rear cover and the rear ring wall, causing a large gradient of shear stress at that location. The shear stress of molten salt at 300 °C is significantly higher than that of the pure and molten

salt at 565 °C, while the viscosity and shear stress distribution of the pure water and molten salt at 565 °C are quite similar.

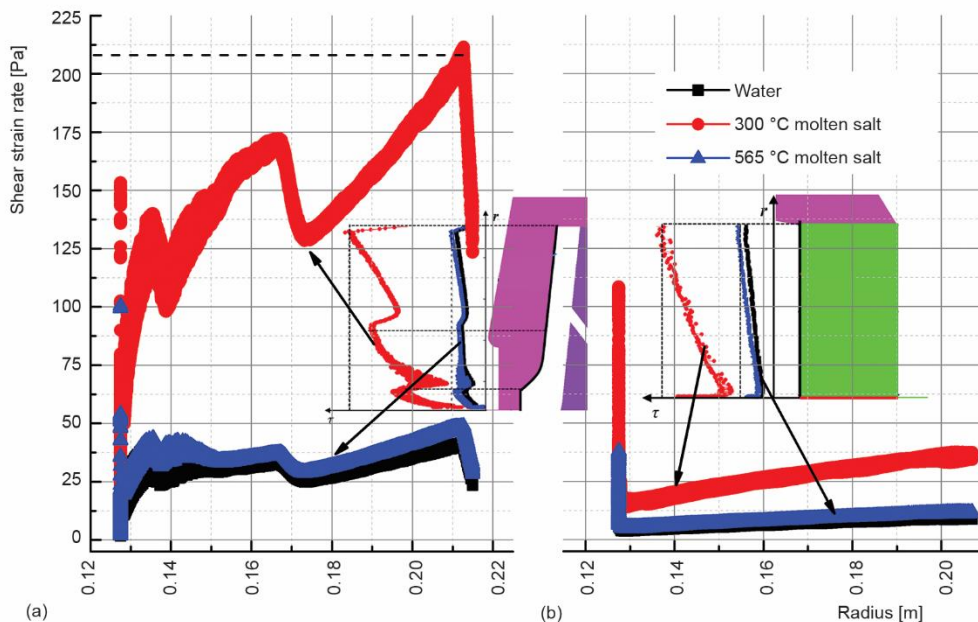


Figure 16. Distributions of the shear stress on shroud; (a) shear stress on front shroud, (b) shear stress on rear shroud

The maximum shear strain rates on the front shroud wall are 46882.99 s^{-1} , 64296.95 s^{-1} , and 42772.86 s^{-1} , and the shear stresses are 41.78 Pa, 208.07 Pa, and 49.47 Pa

for different media, respectively. The ratios of the shear stress to shear strain rate are, 0.000891, 0.003236, and 0.001157, respectively. The shear strain rates at the maximum radius of the rear shroud wall are 10540.80 s^{-1} , 11494.59 s^{-1} , and 10403.15 s^{-1} , respectively, and the shear stresses are 8.89 Pa, 37.29 Pa, and 12.06 Pa, respectively. The ratios of the shear stress to shear strain rate are 0.000843, 0.003244, and 0.001159, respectively. The ratio of the shear stress to the strain rate on front and rear shroud wall is consistent, and the results are highly correlated with the viscous properties of the three media, which indicates that the shear stress of front and rear shroud wall is mainly affected by viscous properties. According to the correlations among the shear strain rate, shear stress, energy loss and the pump cavity boundary of the shroud wall, the width of the pump chamber should be reasonably controlled in design.

Conclusions

The flow structures of the MSP under designed condition were calculated with the pure water, molten salt at $300 \text{ }^\circ\text{C}$ and molten salt at $565 \text{ }^\circ\text{C}$, with special emphasis on the flow field and the disk friction loss inside the first stage using the experimental and numerical simulations. The main findings are concluded as follows.

- By the experiments and simulations with the pure water, the results show that the change of the dielectric properties has little effect on the pump head, but the increase of the medium viscosity will slightly reduce the pump efficiency.
- The density and viscosity of the three medium have a relatively weak influence on the velocity distribution of the flow field, but the medium viscosity can produce a great viscous friction loss in the impeller channel and reduce the relative velocity in the impeller chamber. With the correlated analysis among three medium, it can be seen that viscosity is the main factor affecting the distributions of the shear stress; leakage is weakly affected by the physical properties; the design of the gap between the mouth and ring of the MSP under different temperature conditions only needs to consider the deformation caused by the high temperature.
- By the analysis of the disk friction loss in the first stage, it is found that the higher the percentage of energy loss is, the higher the viscosity is, as well as the density, indicating that the disk friction loss is affected by both the viscosity and the density of the medium. According to the correlation among the shear strain rate, shear stress, energy loss and the pump cavity boundary of the shroud wall, the width of the pump chamber should be reasonably controlled in design. Simultaneously, avoiding mutations in the pump chamber boundary is beneficial to reduce the shear stress and the disk loss energy.

Acknowledgment

This work is supported by the Scientific and Technological Achievements Translate Foundation of Jiangsu Province (Grant No. BA20116167), Innovation Project for Postgraduates of Jiangsu Province (Grant No. KYCX17_1772), 333 Project of Jiangsu Province (Grant No. 2016III-2731), Six Talent Peaks Project in Jiangsu Province (Grant No. HYG-008) and Qing Lan Project.

References

- [1] Hunt, J. Handling Molten salt for Sun Power, *World Pumps*, 1 (2011), Jan., pp. 22-26
- [2] Ortega, J. I., Burgaleta, J. I., Téllez F M. Central Receiver System Solar Power Plant Using Molten Salt as Heat Transfer Fluid, *Journal of Solar Energy Engineering*, 130 (2008), 2, pp. 247-266
- [3] Zavoico, A. B., Solar Power Tower Design Basis Document, Revision 0, Office of Scientific & Technical Information Technical Reports, Sandia National Laboratory, Albuquerque, N. Mex., USA, 2001

- [4] Nunes, V. M. B., et al., Viscosity of Molten Sodium Nitrate, *International Journal of Thermophysics*, 27 (2006), 6, pp. 1638-1649
- [5] Roberto, S. L., et al., Molten Salts Database for Energy Applications, *Chemical Engineering & Processing Process Intensification*, 73 (2013), Nov., pp. 87-102
- [6] Nunes, V. M. B., et al., Molten Salts as Engineering Fluids – A Review : Part I. Molten Alkali Nitrates, *Applied Energy*, 183 (2016), Dec., pp. 603-611
- [7] Chen, Y. C., et al. Experimental Study of Viscosity Characteristics of High-Temperature Heat Transfer Molten Salts, *Science China Technological Sciences*, 54 (2012), Aug., ID 3022
- [8] Cheng, W. J., et al., Numerical Analysis of Unsteady Flow in Molten Salt Pump for Different Viscosities, *Journal of Nanjing Tech University*, 37 (2015), 5, pp. 102-107
- [9] Xiao, C., et al., Effects of Molten Salt Density on the Performances of Molten Salt Pump, *Light Industry Machinery*, 32 (2014), 4, pp. 5-8
- [10] Daily, J. W., et al., Chamber Dimension Effects on Induced Flow and Frictional Resistance of Enclosed Rotating Disks, *Journal of Basic Engineering*, 82 (1960), 1, ID 217
- [11] Li, W. G., Effects of Viscosity of Fluids on Centrifugal Pump Performance and Flow Pattern in the Impeller, *International Journal of Heat & Fluid Flow*, 21 (2000), 2, pp. 207-212
- [12] Shao, C. L., et al., Experiment and Numerical Simulation of External Performances and Internal Flow of a Molten Salt Pump, *Journal of Aerospace Power*, 31 (2016), 8, pp. 1935-1942
- [13] Yang, M. G., et al., Interior Flow and Unsteady Performance of Molten Salt Pump with Splitter Space Guide Vane, *Journal of Drainage and Irrigation Machinery Engineering*, 33 (2015), 4, pp. 306-310
- [14] Li, Y. X., et al., Influence of Volute Structure on Performance of Vertically-Installed High-Temperature Molten-Salt Pump, *Journal of Chemical Industry and Engineering*, 64 (2013), 8, pp. 2853-2859
- [15] Guan, X. F., Modern Pumps Theory and Design, *China Aerospace Press*, Beijing, 2011
- [16] Gao, B., et al., Effect of Wear-Ring Clearance on Performance and Flow Characteristics of Centrifugal Pump, *Journal of drainage and irrigation machinery engineering*, 35 (2017), 1, pp. 13-17
- [17] Shi, W. D., et al., Influence on Performance of Submersible Well Pump Changing Clearance of Wear-Rings, *Journal of Drainage & Irrigation Machinery Engineering*, 118 (2013), 1, pp. 69-73
- [18] Gulich, J. F., *Centrifugal Pumps*, Springer-Verlag, Berlin, Germany, 2014